

Symmetry, Disorder and Transport Through Altermagnetic Quantum Dots and Their Antiferromagnetic Twins

George Kirczenow¹

¹Department of Physics, Simon Fraser University, Burnaby, British Columbia, Canada V5A 1S6

(Dated: February 10, 2026)

Altermagnetic crystals resemble antiferromagnets in that they have no macroscopic magnetization, but unlike antiferromagnets they exhibit spin-split band structures. Here the transport properties of altermagnetic quantum dots and their antiferromagnetic twins are explored theoretically for the first time with the help of Landauer-Büttiker theory, symmetry considerations and tight-binding models. The influence of the symmetries of the quantum dots, their parent crystal lattices, their shapes and edges, lead arrangements and disorder on the anomalous Hall effect, the spin-Hall effect and spin filtering by the quantum dots are investigated.

I. INTRODUCTION

Altermagnets, in common with antiferromagnets, have compensated antiparallel magnetic ordering at the atomic scale and thus have no overall macroscopic magnetization. However, in common with ferromagnets but unlike antiferromagnets, they have spin-split band structures in reciprocal space.¹ This difference between altermagnets and antiferromagnets is related to differing symmetry operations connecting the crystal sublattices of opposite spin in these two classes of materials.^{2–9} The transport phenomena exhibited by altermagnets include the anomalous Hall effect (a transverse voltage induced by an electric current in absence of any applied magnetic field)^{10–21} the spin-Hall effect^{1,22–30,32–36} and non-relativistic spin currents.^{23–31,34,37–39}

These phenomena in *macroscopic* altermagnetic crystals are attracting intense theoretical and experimental interest.¹ However, little or nothing is known regarding potential analogs of the anomalous Hall effect and the spin-Hall effect or non-relativistic spin currents in ultra small altermagnetic structures, i.e., in quantum dots. Important open questions concern the roles of the quantum dot's geometry, its symmetries, its parent crystal lattice, its shape and structure of its edges, any defects or disorder that may be present, and the configuration of leads that should be attached to the quantum dot for studies of quantum dot transport.

This paper initiates the theoretical exploration of these issues by considering tight binding models that have recently been proposed by Zhu *et al.*⁷ and Che *et al.*⁸ as vehicles for investigating the fundamental physics of macroscopic altermagnetic crystals in relation to their real space symmetries. Here these models are adapted to describe nanoscale altermagnetic quantum dots with $C_4\mathcal{T}$ symmetry and their antiferromagnetic twins with \mathcal{IT} symmetry. An example of both is shown in Fig. 1. Here C_4 , \mathcal{I} and \mathcal{T} are the spatial fourfold rotation, inversion and time reversal operations respectively. Transport through such quantum dots in two terminal and four terminal configurations is modeled here by attaching non-magnetic ideal tight binding leads to the quantum dot. The relevant transport coefficients, namely, the anomalous Hall resistance, the spin-Hall conductance and the spin filtering efficiency, are calculated within the Büttiker-Landauer formalism^{40–42} after evaluating the Landauer lead-to-lead electron quantum transmission probabilities by solving the relevant Lippmann-

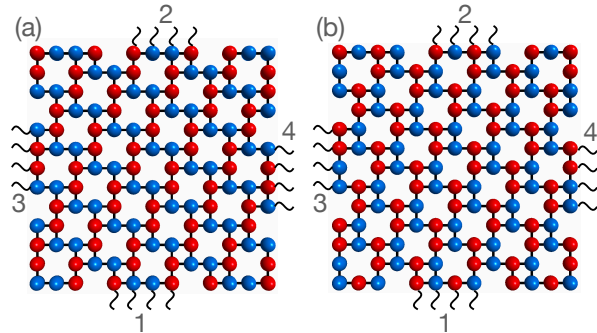


Figure 1. (Color online). (a) An altermagnetic model quantum dot and leads with $C_4\mathcal{T}$ symmetry and (b) its antiferromagnetic twin and leads with \mathcal{IT} symmetry. Red (blue) disks are sites with up (down) out of plane local spins. Wavy lines represent one dimensional ideal conductors (modeled as tight binding chains) each carrying a spin up and a spin down conducting channel. Four such conductors constitute each electrical lead contacting the quantum dot. In a Hall measurement leads 1 and 2 carry the electric current, leads 3 and 4 carry no current, and the Hall voltage drop is measured between leads 3 and 4. The quantum dots (a) and (b) are fragments of the altermagnetic and antiferromagnetic 1/5-depleted square lattice bulk crystals discussed in Ref. 7, respectively. The dot edges are of the armchair type. Images prepared using Macmolpt software.⁴³

Schwinger equations that describe electron scattering through the quantum dot. These quantum transport calculations are carried out in the linear response regime for quantum dot geometries based on the 1/5-depleted square lattice,⁷ the square-octagon lattice⁷ and the Lieb lattice⁸ with arm-chair, zigzag, square or octagon edges and various lead arrangements, conforming to $C_4\mathcal{T}$ or \mathcal{IT} symmetries. The effects of disorder in the quantum dots and symmetry breaking lead arrangements are also investigated.

The new results reported here are as follows:

If the complete system of the altermagnetic quantum dot together with the four leads attached to it in the Hall geometry is symmetric under the operation $C_4\mathcal{T}$ as in Fig. 1(a) then there is no anomalous Hall effect. I.e., in the 4-lead Hall geometry there is no potential difference between the two voltage leads when they carry no current while a current flows through the two current leads. This finding is shown here to be a consequence of the $C_4\mathcal{T}$ symmetry. However, the antiferromag-

netic twin of this system (that has the same atomic structure but whose distribution of local spins is symmetric under the operation \mathcal{IT} as in Fig.1(b)) does exhibit the anomalous Hall effect. Moreover, this antiferromagnetic quantum dot exhibits giant Hall resistances in the tunneling regime.

Also, the altermagnetic quantum dot and its antiferromagnetic twin are predicted here to exhibit a spin-Hall effect provided that the nanostructure consisting of the dot and leads does not have mirror symmetry. In these systems the spin-Hall effect manifests itself as pure spin currents in the Hall voltage leads that carry no net electric currents.

If the Hall leads are removed from these systems and only the current leads are retained in the same geometry as above, then the altermagnetic quantum dot is predicted here to act as an efficient electron spin filter whereas its antiferromagnetic twin is predicted to exhibit no spin filtering due to its \mathcal{IT} symmetry.

Finally, if all of the symmetries of these systems are broken by introducing disorder into the quantum dot or appropriately altering the lead geometries, both the altermagnetic quantum dots and their antiferromagnetic twins are predicted to exhibit the anomalous Hall effect, the spin-Hall effect and spin filtering.

The remainder of this paper is organized as follows: The Hamiltonian and formalism used to calculate the transport properties of altermagnetic and antiferromagnetic quantum dots are described in Sec. II. Altermagnetism and antiferromagnetism in quantum dots are discussed in Sec. III A. The anomalous Hall effect, the spin-Hall effect and spin filtering by altermagnetic and antiferromagnetic 1/5-depleted square lattice quantum dots with armchair edges are discussed in Secs. III B, III C and III D, respectively. Other quantum dot edge and lead geometries are discussed in Sec. III E. Quantum dots with mirror symmetries are discussed in Sec. III F. Effects of disorder in quantum dots on transport are addressed in Sec. III G. Symmetry breaking leads are discussed in Sec. III H. The main findings of this work are summarized in Sec. IV.

II. METHOD

A minimal model Hamiltonian⁷ for the altermagnetic and antiferromagnetic quantum dots considered in this paper is:

$$H = -t \sum_{\langle ij \rangle} (a_{i\uparrow}^\dagger a_{j\uparrow} + a_{i\downarrow}^\dagger a_{j\downarrow}) - J \sum_i S_i (a_{i\uparrow}^\dagger a_{i\uparrow} - a_{i\downarrow}^\dagger a_{i\downarrow}) \quad (1)$$

where $a_{i\uparrow}^\dagger$ creates a spin up electron on site i of the quantum dot, $\langle ij \rangle$ indicates nearest neighbor sites i and j , and $S_i = S$ for local spin up at site i and $S_i = -S$ for local spin down at site i . In this work the atomic chains making up the leads are represented by Hamiltonian

$$H_C = -t_C \sum_{\langle ij \rangle} (b_{i\uparrow}^\dagger b_{j\uparrow} + b_{i\downarrow}^\dagger b_{j\downarrow}) \quad (2)$$

where $b_{i\uparrow}^\dagger$ creates a spin up electron on site i of the chain. These atomic chains are non-magnetic since there is no en-

ergy splitting between spin up and down states in H_C . It is assumed throughout this paper that the spin up and down states traveling through the leads towards the quantum dot are equally populated with electrons and that the temperature is zero Kelvin.

In this work calculation of the transport coefficients of quantum dots described by Eq. 1 and 2 proceeds by solving the Büttiker equations⁴⁰

$$I_i = \frac{q_e}{h} (N_i \mu_i - R_{ii} \mu_i - \sum_{j \neq i} T_{ij} \mu_j), \quad (3)$$

where I_i is the electric current in lead i , μ_i is the electrochemical potential of lead i , T_{ij} is the electron transmission probability from lead j to lead i , and R_{ii} is the electron reflection probability from the quantum dot in lead i , N_i is the total number of spin up and spin down conducting channels supported by lead i and q_e is the electron charge.

The electron transmission and reflection probabilities T_{ij} and R_{ii} are found by numerically solving the Lippmann-Schwinger equations

$$|\psi^m\rangle = |\phi_\circ^m\rangle + G_\circ(E)W|\psi^m\rangle, \quad (4)$$

as is described in Appendix A of Ref. 44. Here $|\phi_\circ^m\rangle$ is an eigenstate of the m^{th} lead that is decoupled from the quantum dot, $G_\circ(E)$ is the sum of the Green's functions of the quantum dot and leads when they are decoupled, and $|\psi^m\rangle$ is the scattering eigenstate of the coupled system. W is the coupling between the quantum dot and the ideal leads, i.e.,

$$W = - \sum_n t_C (b_{n\uparrow}^\dagger a_{n\uparrow} + b_{n\downarrow}^\dagger a_{n\downarrow} + H.c.) \quad (5)$$

where $b_{n\uparrow}^\dagger$ is the electron creation operator at a lead site attached to the quantum dot, $a_{n\uparrow}$ is the electron annihilation operator at the quantum dot site attached to the corresponding lead, and the hopping amplitude t_C is assumed for simplicity to be the same as the hopping between the sites of the chains that make up the leads. Having evaluated scattering states $|\psi^m\rangle$, the coefficients T_{ij} that enter Büttiker equations (Eq.3) are given by

$$T_{ij}(E) = \sum_{l,p} |t_{lp}^{ij}|^2 \frac{v_l^i}{v_p^j}, \quad (6)$$

where t_{lp}^{ij} is the quantum transmission amplitude of an electron transmitted from the p^{th} chain of lead j to the l^{th} chain of lead i at energy E obtained from the scattering states $|\psi^m\rangle$. $v_{l(p)}^{i(j)} = \frac{1}{\hbar} \frac{\partial \epsilon}{\partial k}$ is the electron velocity in the 1-D semi-infinite chain $l(p)$ of lead $i(j)$ at energy E , and ϵ are the energy eigenvalues of the tight-binding Hamiltonian of the semi-infinite ideal chain.

To calculate the Hall resistance R_H of a quantum dot, following the calculation of electron transmission probabilities T_{ij} at the Fermi energy E_F , the Büttiker equations Eq. (3) are solved for the potential difference $\Delta V_{3,4}$ between the voltage

contacts 3 and 4 subject to the condition of zero electric current in the voltage leads, i.e., $I_3 = I_4 = 0$. Then

$$R_H = \frac{\Delta V_{3,4}}{I_{1,2}}, \quad (7)$$

where $I_{1,2}$ is the electric current flowing between the current contacts 1 and 2 and; the numbering of the contacts is as in Fig.1. Here the potential difference ΔV and electrochemical potentials μ appearing in the Büttiker equations Eq. (3) are related by $\Delta V = \Delta\mu/q_e$.

Having found the electrochemical potentials μ_i for which the electric currents in the Hall voltage leads are zero, $I_3 = I_4 = 0$, the spin-Hall effect is investigated here as follows: For the values of the electrochemical potentials μ_i for which the electric currents in the Hall voltage leads are zero the spin-resolved version of the Büttiker equations (3) is used to evaluate the spin-resolved electric currents $I_{i\uparrow}$ and $I_{i\downarrow}$ in the leads. Then the spin current I_i^s in voltage lead i is defined as²²

$$I_i^s = \frac{\hbar}{2q_e}(I_{i\uparrow} - I_{i\downarrow}) \quad (8)$$

A non-zero spin current I_i^s in a voltage lead where the total electric current is zero is a manifestation of the spin-Hall effect.

In this work in order to address spin filtering in 2-terminal geometries a spin-unpolarized electron flux is considered to enter the quantum dot through the electron source lead. Then the spin resolved probabilities T_{\uparrow} and T_{\downarrow} of spin up and spin down electrons exiting through the drain lead at the Fermi energy are calculated. T_{\uparrow} and T_{\downarrow} are obtained by restricting the sum over l in Eq. (6) to spin up and spin down states, respectively, while including both the spin up and spin down states in the sum over p . The axis of quantization is perpendicular to the plane of the quantum dot. The spin filtering efficiencies are then defined as

$$F_{\uparrow} = T_{\uparrow}/(T_{\uparrow} + T_{\downarrow}) \quad (9)$$

$$F_{\downarrow} = T_{\downarrow}/(T_{\uparrow} + T_{\downarrow}) \quad (10)$$

For the present transport calculations the parameter values in Eq. (1) are chosen to be $t = 1\text{eV}$ and $JS = 0.5\text{eV}$ as in Ref. 7 for sites with local spins. For sites with no local spin $JS = 0$. The parameter t_C in Eqs. 2 and 5 has been chosen to be 2.0 eV . This choice ensures that the full spectrum of the quantum dot energy eigenstates falls well within the bandwidth of the tight binding chains that make up the leads that carry electrons into and out of the quantum dots.

III. RESULTS

A. Altermagnetic and Antiferromagnetic Quantum Dots

The quantum dots in Fig.1 (a) and (b) are fragments of 1/5-depleted square lattice bulk crystals with $C_4\mathcal{T}$ and \mathcal{IT} symmetries, respectively. As has been pointed out in Ref. 7,

those bulk crystals are altermagnetic and antiferromagnetic, respectively. This finding of Ref. 7 has been confirmed by band structure calculations carried out for these bulk crystals as a part of the present work, i.e., the bulk crystals with $C_4\mathcal{T}$ symmetry are found to exhibit spin split electronic bands and thus are altermagnetic, whereas those with \mathcal{IT} symmetry do not and are thus antiferromagnetic. Accordingly, the quantum dots in Fig.1 (a) and (b) will be referred to as altermagnetic and antiferromagnetic, respectively.

The nanostructures in Fig.1 (a) and (b) are fully symmetric under the operations $C_4\mathcal{T}$ and \mathcal{IT} , respectively. This applies to the quantum dots themselves, including their edges, as well as to the non-magnetic leads. These complete symmetries are decisive in determining the transport properties of these systems, as will be seen below.

B. Anomalous Hall Effect

1. Altermagnetic Quantum Dot

For the altermagnetic quantum dot in Fig.1 (a) the numerical calculations described in Section II were carried out choosing leads 1 and 2 to be the current leads and leads 3 and 4 to be the voltage leads that carry no current. The result was $R_H = 0$, i.e., zero Hall resistance defined by Eq. (7) (and zero Hall voltage) for all values of the electron Fermi energy.

This absence of an anomalous Hall effect can be understood as a direct consequence of the $C_4\mathcal{T}$ symmetry of the altermagnetic quantum dot and leads in Fig.1 (a), as will be explained next:

In the absence of magnetic fields, electron lead to lead transmission probabilities obey $T_{ij} = T_{ji}$ for all leads i and j due to time reversal symmetry.⁴⁰ However, the $C_4\mathcal{T}$ symmetry of Fig.1 (a) implies additional symmetries of the transmission and reflection probability matrices T_{ij} and R_{ii} and of N_i the total number of conducting channels supported by each lead. Namely,

$$N_1 = N_2 = N_3 = N_4 \equiv N \quad (11)$$

$$R_{11} = R_{22} = R_{33} = R_{44} \equiv R \quad (12)$$

$$T_{12} = T_{21} = T_{34} = T_{43} \equiv Z \quad (13)$$

$$T_{13} = T_{31} = T_{24} = T_{42} = T_{14} = T_{41} = T_{23} = T_{32} \equiv T \quad (14)$$

Setting $I_3 = I_4 = 0$ for the currents in the voltage leads and solving the Büttiker equations (3)⁴⁰ subject to the symmetry constraints (11-14) yields $\mu_3 = \mu_4 = T(\mu_1 + \mu_2)/(N - R - Z)$. Applying the charge conservation condition $N = R + Z + 2T$, this reduces to

$$\mu_3 = \mu_4 = (\mu_1 + \mu_2)/2. \quad (15)$$

This means that there is no potential difference between the two voltage leads 3 and 4 and hence no anomalous Hall effect.

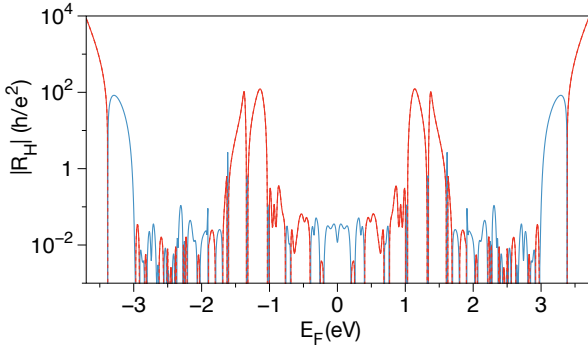


Figure 2. (Color online). Absolute values of the Hall resistance vs. electron Fermi energy of the antiferromagnetic nanostructure in Fig.1 (b). Positive (negative) values of R_H are shown in red (blue).

This can be understood intuitively as following from the symmetries between leads 3 and 4 expressed by Eq. (11-14). For example, the condition (14) that $T_{31} = T_{41}$ means that electrons entering the dot from lead 1 are scattered equally into voltage leads 3 and 4 so that cancelation of the associated net currents flowing in leads 3 and 4 can be accomplished by applying equal voltages to leads 3 and 4.

Thus the $C_4\mathcal{T}$ symmetry that results in altermagnetism in a 1/5-depleted square lattice bulk crystal⁷ suppresses the anomalous Hall effect in an altermagnetic quantum dot that, together with its leads, obeys $C_4\mathcal{T}$ symmetry. It is worth noting that since the structure in Fig.1 (a) does not have mirror symmetry between the voltage contacts 3 and 4, it is clearly the $C_4\mathcal{T}$ symmetry together with time reversal symmetry $T_{ij} = T_{ji}$ ⁴⁰ that is responsible for the absence of the anomalous Hall effect. Since this result is purely a consequence of symmetry it holds for all values of the Fermi energy.

2. Antiferromagnetic Quantum Dot

The antiferromagnetic quantum dot and leads in Fig.1 (b) have \mathcal{IT} symmetry, a lower symmetry than that of the $C_4\mathcal{T}$ -symmetric altermagnetic structure in Fig.1 (a). Thus not all of the symmetries expressed by Eq. (12-14) apply. For example, $T_{31} = T_{41}$ does *not* hold for the antiferromagnetic quantum dot and leads. Consequently an electron entering the dot from current lead 1 is scattered with unequal probabilities into voltage leads 3 and 4. Thus in order for the net electric currents in the voltage leads to be zero ($I_3 = I_4 = 0$) unequal potentials need to be applied to the two voltage leads. Thus the antiferromagnetic quantum dot in Fig.1 (b) exhibits an anomalous Hall effect. For this system the Hall resistance R_H given by Eq. (7) has been computed as described in Section II and the result is shown in Fig.2 where positive (negative) values of R_H are shown in red (blue).

As is seen in Fig.2, the sign of the Hall resistance depends on the value of the Fermi energy and R_H exhibits many resonances that are due in part to the influence of the discrete spectrum of the dot on transport. Giant values of R_H are seen

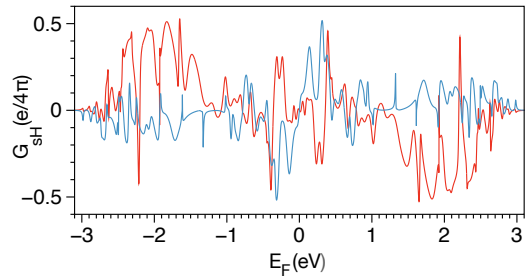


Figure 3. (Color online). Spin-Hall conductance vs. electron Fermi energy of the altermagnetic (antiferromagnetic) nanostructure in Fig.1 (a) (Fig.1 (b)) shown in red (blue).

in Fig.2 for Fermi energies E_F such that $|E_F| > 3\text{eV}$ and $1\text{eV} < |E_F| \lesssim 1.5\text{eV}$. This can be interpreted as follows:

In these energy ranges the density of states for the bulk antiferromagnet of which the quantum dot in Fig.1 (b) is a fragment, vanishes. Thus transport through the quantum dot at these energies occurs by quantum tunneling. Now consider an electron entering the dot through current lead 1. To exit the dot through current lead 2 and thus to contribute to the current through the dot the electron has to tunnel further than it has to in order to reach voltage lead 3 or 4. For this reason the electric current through the dot decreases more rapidly than the Hall voltage as the Fermi energy moves more deeply into the tunneling regime. Thus the Hall resistance $R_H = \frac{\Delta V_{3,4}}{I_{1,2}}$ grows exponentially. For example, as the Fermi energy descends to progressively lower values below -3eV in Fig.2 the absolute value of the anomalous Hall resistance is seen to increase by more than 6 orders of magnitude.

C. Spin-Hall Effect

For the altermagnetic quantum dot of Fig.1(a), for values of the lead electrochemical potentials μ_i that satisfy Eq. (15) so that the electric currents in the voltage leads 3 and 4 vanish ($I_3 = I_4 = 0$), the spin-resolved electric currents $I_{i\uparrow}$ and $I_{i\downarrow}$ in the voltage leads have been calculated as described in Section II. It was found that $I_{3\uparrow} = -I_{3\downarrow}$ and $I_{4\uparrow} = -I_{4\downarrow}$ in linear response for all values of the electron Fermi energy. This means that there is a net spin current I_i^s defined by Eq. (8) in each voltage lead although these leads carry no electric current. Thus the altermagnetic nanostructure in Fig.1 (a) exhibits a spin-Hall effect although it does not support an anomalous Hall effect. The spin currents in voltage leads 3 and 4 of Fig.1 (a) are found to be equal and to travel in the same direction, but the direction depends on the Fermi energy. Fig. 3 shows in red the computed spin-Hall conductance $G_{\text{SH}} = I^s/\Delta V$ where I^s is the spin current in the leads 3 and 4 of Fig.1 (a) and ΔV is the potential difference between leads 1 and 2.

For the antiferromagnetic dot and leads shown in Fig.1(b), the electrochemical potentials μ_i for which the electric currents vanish in the voltage leads ($I_3 = I_4 = 0$) were calculated by solving the Büttiker equations (3). The spin-

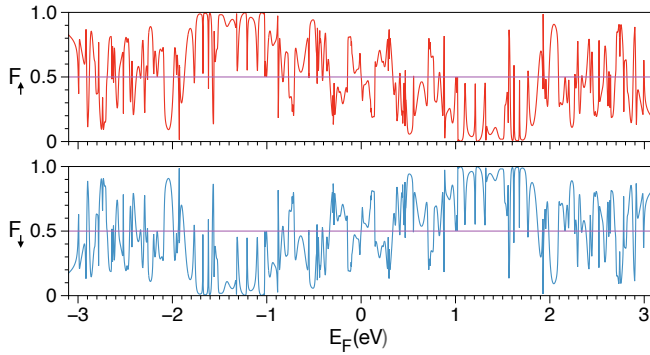


Figure 4. (Color online). Spin filtering efficiencies F_\uparrow (red) and F_\downarrow (blue) vs. electron Fermi energy for the altermagnetic quantum dot in Fig.1(a). F_\uparrow and F_\downarrow for the antiferromagnetic dot in Fig.1 (b) are shown in mauve.

resolved electric currents $I_{i\uparrow}$ and $I_{i\downarrow}$ in the voltage leads were then calculated as described in Section II. It was found that $I_{3\uparrow} = -I_{3\downarrow}$ and $I_{4\uparrow} = -I_{4\downarrow}$. Thus (as for the altermagnetic dot) there is a net spin current I_i^s defined by Eq. (8) in each voltage lead although these leads carry no electric current. The spin currents I_i^s in the two voltage leads are equal in magnitude but flow in opposite directions which depend on the Fermi energy. The spin-Hall conductance $G_{\text{SH}} = I^s/\Delta V$ for a voltage lead of Fig.1 (b) is shown in blue in Fig. 3.

Thus both the altermagnetic and antiferromagnetic quantum dots exhibit the spin-Hall effect and both can in principle be used as sources of pure spin currents in Hall voltage leads that carry no electric current.

D. Spin Filtering

In order to study spin filtering by altermagnetic and antiferromagnetic quantum dots in two-terminal geometries, the current leads 1 and 2 in Fig.1 (a) and (b) are retained while leads 3 and 4 are removed. Both spin up and spin down electrons are assumed to flow towards the dot equally through lead 1. The spin resolved probabilities T_\uparrow and T_\downarrow of spin up and spin down electrons exiting through lead 2 at the Fermi energy and the spin filtering efficiencies F_\uparrow and F_\downarrow have been computed numerically as described at the end of Section II.

The results for the altermagnetic quantum dot are shown in red and blue in Fig. 4. The altermagnetic quantum dot is found to exhibit nearly perfect spin filtering, i.e., $F_\uparrow \approx 1$ or $F_\downarrow \approx 1$ in some ranges of the Fermi energy. By contrast, the antiferromagnetic dot displays no spin filtering at all. For it F_\uparrow and F_\downarrow (shown in mauve) are both 0.5 at all energies.

This difference between the altermagnetic quantum dot and its antiferromagnetic twin can be understood as follows:

Application of the symmetry operation \mathcal{IT} of the antiferromagnetic dot transforms lead 2 into lead 1 and spin up into spin down (and vice versa). It follows that

$$T_{2\uparrow 1\uparrow} = T_{1\downarrow 2\downarrow}, \quad (16)$$

i.e., the transmission probability of a spin up electron from

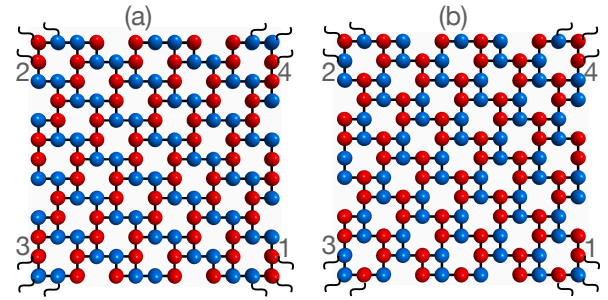


Figure 5. (Color online). Quantum dots (a) and (b) are fragments of the altermagnetic and antiferromagnetic 1/5-depleted square lattice bulk crystals respectively, as in Fig.1 but with leads attached to the corners of the dots, while preserving the overall $C_4\mathcal{T}$ symmetry and \mathcal{IT} symmetry, respectively. Notation as in Fig.1.

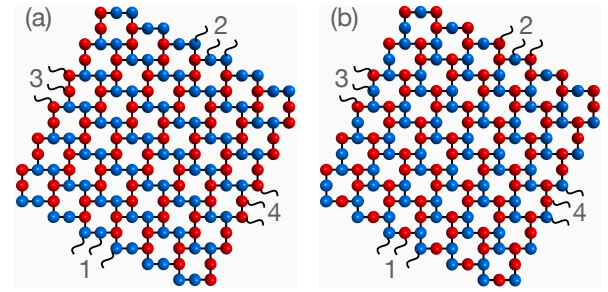


Figure 6. (Color online). Quantum dots (a) and (b) are fragments of the altermagnetic and antiferromagnetic 1/5-depleted square lattice bulk crystals respectively, as in Fig.1 but with zigzag edges, still preserving the overall $C_4\mathcal{T}$ symmetry and \mathcal{IT} symmetry, respectively. Notation as in Fig.1.

lead 1 to lead 2 equals the transmission probability of a spin down electron from lead 2 to lead 1. Noting that the Hamiltonian in Section II is diagonal in spin, time reversal symmetry applied to only the spatial part of the wave function implies that

$$T_{1\downarrow 2\downarrow} = T_{2\downarrow 1\downarrow} \quad (17)$$

Eq. (16) and (17) together yield $T_{2\uparrow 1\uparrow} = T_{2\downarrow 1\downarrow}$. I.e., The transmission probability of a spin up electron from lead 1 to lead 2 equals that for a spin down electron. Since the Hamiltonian in Section II is diagonal in spin this means that there cannot be any spin filtering.

This argument does not hold for the altermagnetic quantum dot since for it the symmetry operation that connects leads 1 and 2 is not \mathcal{IT} but $(C_4\mathcal{T})^2 = \mathcal{I}$ which does not flip the electron's spin. Therefore the symmetry of the altermagnetic quantum dot does not require the transmission probability of a spin up electron from lead 1 to lead 2 to equal that for a spin down electron, so spin filtering is allowed as is seen in Fig. 4.

E. Other Symmetric Quantum Dot and Lead Arrangements

Fig.5 (a) and (b) show the same altermagnetic and antiferromagnetic quantum dots as those of Fig.1 (a) and (b) respec-

tively, but with leads attached to the corners of the dots. The dots with these lead geometries have the same the overall $C_4\mathcal{T}$ and \mathcal{IT} symmetries, respectively, as Fig.1 (a) and (b). Fig.6 (a) and (b) show dots with zigzag edges. They are different fragments of the altermagnetic and antiferromagnetic 1/5-depleted square lattice bulk crystals, respectively, than those of Fig.1 but these dots and leads also have the same the overall $C_4\mathcal{T}$ and \mathcal{IT} symmetries, respectively.

The present numerical transport calculations for the altermagnetic dot/lead arrangements in Fig.5 (a) and Fig.6 (a) show that they do not exhibit an anomalous Hall effect but do exhibit a spin-Hall effect, and also spin filtering in a two terminal arrangement. The antiferromagnetic structures in Fig.5 (b) and Fig.6 (b) are found to exhibit an anomalous Hall effect with giant Hall resistance, a spin-Hall effect, and no two-terminal spin filtering. This behavior is similar to that described above for the corresponding nanostructures in Fig.1. This finding suggests that these transport effects are governed by the $C_4\mathcal{T}$ and \mathcal{IT} symmetries of the dots and leads, and that provided that these symmetries are obeyed, other details such as the specific shapes of the dots and lead arrangements are not crucial. However, the systems considered above do not have any mirror symmetries. These and their influence on transport will be addressed next.

F. Quantum Dots with Mirror Symmetries

Fig.7 (a) and Fig.8 (a) show altermagnetic quantum dots that are fragments of square-octagon lattice⁷ and Lieb lattice⁸ bulk crystals, respectively. These dots and their leads have the $C_4\mathcal{T}$ symmetry but in addition they are mirror-symmetric. Their axes of reflection bisect them both horizontally and vertically. Like the other altermagnetic quantum dots discussed above, the present study has found these systems to not exhibit an anomalous Hall effect, but to support 2-terminal spin filtering if leads 3 and 4 are removed. However, unlike the other altermagnetic quantum dots discussed above these systems do not exhibit a spin-Hall effect. If the mirror symmetries in Fig.7 (a) and Fig.8 (a) are broken while retaining the $C_4\mathcal{T}$ symmetry by shifting all of the leads clockwise or counter-clockwise by the same amount along the dot's edges, the spin-Hall effect is recovered while the anomalous Hall effect remains absent and 2-terminal spin filtering is retained. Thus it is reasonable to conclude that the mirror symmetries are responsible for the suppression of the spin-Hall effect in these systems. This conclusion is consistent with the finding of the present numerical calculations that the antiferromagnetic twin quantum dots/leads in Fig.7 (b) and Fig.8 (b) (that are symmetric under \mathcal{IT} but have no mirror symmetries) exhibit the spin-Hall effect and anomalous Hall effect but not two terminal spin filtering, just like the antiferromagnetic quantum dots in Figs.1, 5 and 6 discussed above.

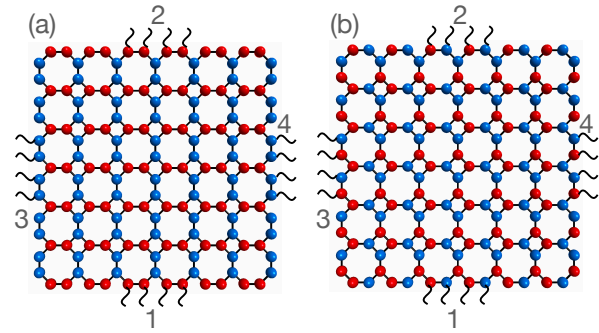


Figure 7. (Color online). Quantum dots (a) and (b) are fragments of altermagnetic and antiferromagnetic square-octagon lattice⁷ bulk crystals, respectively. These dots and their leads have overall $C_4\mathcal{T}$ and \mathcal{IT} symmetries, respectively. Dot edges are of the octagon type. Notation as in Fig.1.

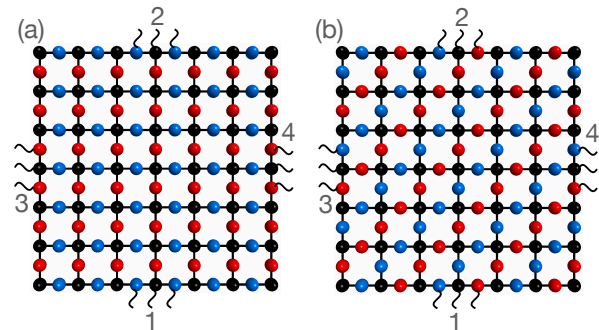


Figure 8. (Color online). Quantum dots (a) and (b) are fragments of altermagnetic and antiferromagnetic Lieb lattice⁸ bulk crystals respectively. These dots and their leads have overall $C_4\mathcal{T}$ symmetry and \mathcal{IT} symmetries, respectively. Red, blue and black disks represent sites with up, down and no local spins. Dot edges are of square type. Notation as in Fig.1.

G. Disordered Altermagnetic and Antiferromagnetic Quantum Dots

The results presented above are for ideal quantum dots and leads that are perfectly symmetric under $C_4\mathcal{T}$ or \mathcal{IT} operations and that in some cases also have mirror symmetries. However, it is also of interest to know how the transport phenomena are affected if symmetry-breaking disorder is present. To this end the effects of disorder modeled by replacing up and down local local spins at random sites by no-spin sites (where $JS = 0$) are examined below. Representative examples where $\sim 20\%$ of the local up (red) and down (blue) spins of altermagnetic and antiferromagnetic fragments of square-octagon lattices⁷ are randomly replaced by no spin (black) sites are shown in Fig.9 (a) and (b) respectively.

1. Anomalous Hall Effect

The calculated anomalous Hall resistances for the disordered altermagnetic and antiferromagnetic quantum dots in

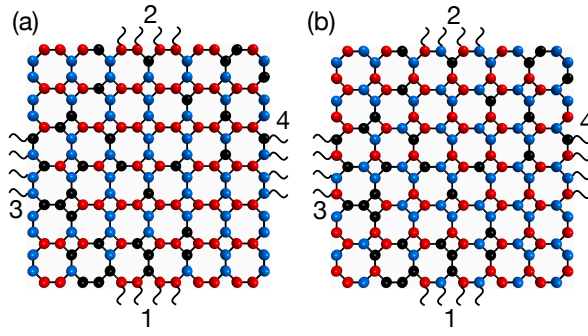


Figure 9. (Color online). Quantum dots (a) and (b) are defective fragments of altermagnetic and antiferromagnetic square-octagon lattice⁷ bulk crystals, respectively. Their respective $C_4\mathcal{T}$ and \mathcal{IT} symmetries and their mirror symmetries are broken by the random substitution of local spins by no-spin defects. Red, blue and black disks represent sites with up, down and no local spins. Notation as in Fig.1.

Fig.9 (a) and (b) are shown in Fig.10 (a) and (b), respectively.

As was discussed above, the anomalous Hall resistance for the ideal altermagnetic dot in Fig.7 (a) is zero for all values of the Fermi energy due to $C_4\mathcal{T}$ symmetry. By contrast, as can be seen in Fig.10 (a), R_H for the disordered altermagnetic dot in Fig.9 (a) is comparable in magnitude to that of its antiferromagnetic twin shown in Fig.10 (b) except around $|E_F| = 1.5\text{eV}$ where the bulk antiferromagnetic crystal has a band gap. Both the disordered altermagnetic dot and its antiferromagnetic twin exhibit giant anomalous Hall resistance for $|E_F| > 3\text{eV}$ where conduction occurs by tunneling. However, the disorder affects the anomalous Hall resistance of the antiferromagnetic dot less drastically, as can be seen by comparing Fig.10 (b) and (c), the disordered and ideal cases, respectively. This is because the $C_4\mathcal{T}$ symmetry of the ideal altermagnetic dot is already broken in the ideal antiferromagnetic dot so that the effects of additional symmetry breaking by disorder are milder: There is some broadening of the prominent anomalous Hall resistance peaks around $|E_F| = 1.5\text{eV}$ in the disordered case (Fig.10 (b)) relative to the ideal case (Fig.10 (c)) as well as reorganization of the fine details of resonance structures.

2. Spin-Hall Effect

As was noted above, for the ideal altermagnetic dot in Fig.7 (a) the spin-Hall conductance is zero due to that structure's mirror symmetry while for its antiferromagnetic twin in Fig.7 (b) there is no mirror symmetry and consequently the spin-Hall effect is present. The calculated spin-Hall conductances for the disordered antiferromagnetic and altermagnetic nanostructures of Fig.9 (b) and (a) are shown in Fig. 11 (a) and (b), respectively. The disorder breaks the mirror symmetries of the altermagnetic nanostructure resulting in the spin-Hall effect that is present in Fig. 11 (b). However, since there is no mirror symmetry even in the ideal antiferromagnetic twin structure, the spin-Hall effect is typically stronger for the disordered antiferromagnetic dot (Fig. 11 (a)) than for the dis-

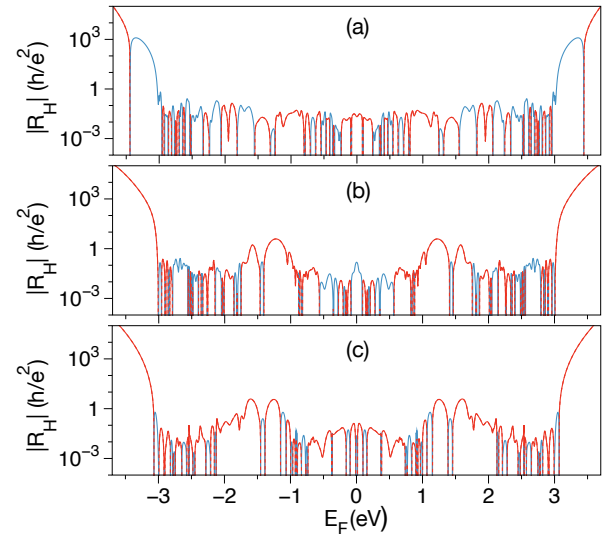


Figure 10. (Color online). Frames (a) and (b) show the absolute values of the Hall resistance vs. electron Fermi energy of the disordered altermagnetic and antiferromagnetic nanostructures in Fig.9 (a) and (b), respectively. Positive (negative) values of R_H are shown in red (blue). Frame (c) shows for comparison the absolute values of the Hall resistance of the pristine antiferromagnetic nanostructure shown in Fig.7 (b).

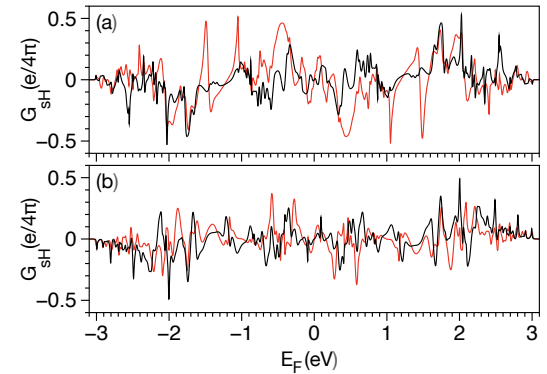


Figure 11. (Color online). Frames (a) and (b) show the spin-Hall conductances vs. electron Fermi energy of the disordered antiferromagnetic and altermagnetic nanostructures of Fig.9 (b) and (a), respectively. Values for spin-Hall conductances in voltage leads 3 and 4 are shown in red and black, respectively.

ordered altermagnetic dot (Fig. 11 (b)). Also, the disorder results in the inequality between the spin-Hall conductances for the two voltage leads shown in red and black in Fig. 11.

3. Spin Filtering

In the two-terminal case where leads 3 and 4 are removed from the disordered antiferromagnetic and altermagnetic quantum dots in Fig.9 the disorder breaks the \mathcal{IT} symmetry of the antiferromagnetic dot in Fig.9 (b). The disordered altermagnetic dot in Fig.9 (a) also does not have \mathcal{IT}

symmetry. Thus according to the reasoning in Sec. III D, in the two-terminal geometry the disordered altermagnetic dot in Fig. 9 (a) and the disordered antiferromagnetic dot in Fig. 9 (b) should both exhibit spin filtering qualitatively similar to that in Fig. 4. This has been confirmed by the present numerical work.

H. Symmetry Breaking Leads

If the configuration of the leads attached to the quantum dot breaks the $C_4\mathcal{T}$ symmetry for an altermagnetic dot or the \mathcal{IT} symmetry for its antiferromagnetic twin, and also all mirror symmetries, then the present work predicts the transport properties of the dot to be qualitatively similar to those of dots with disorder discussed in Sec. III G above.

As an example, consider the Lieb lattice quantum dots in Fig. 8. For the symmetric lead configuration shown in the figure, the altermagnetic dot exhibits no anomalous Hall effect and no spin-Hall effect, but does exhibit spin filtering. The antiferromagnetic dot exhibits an anomalous Hall effect and spin-Hall effect but no spin filtering. However, if lead 2 in Fig. 8 is displaced to the right by even a single atomic site while the other leads are unchanged this breaks the $C_4\mathcal{T}$ symmetry, the \mathcal{IT} symmetry and all mirror symmetries. As a result the altermagnetic dot acquires a giant anomalous Hall resistance similar to that of its antiferromagnetic twin for Fermi energies in the tunneling regime. At other values of the Fermi energy the altermagnetic dot acquires an anomalous Hall resistance that is typically an order of magnitude weaker than that of its antiferromagnetic twin. The broken symmetry also endows the altermagnetic dot with a spin-Hall effect comparable in overall strength to that of its antiferromagnetic twin. With the broken lead symmetry the altermagnetic dot remains a spin filter and its antiferromagnetic twin becomes a spin filter of comparable efficiency.

This sensitivity of transport to a atomic scale displacements of leads is consistent with what is observed experimentally and understood theoretically in other nanoscale systems such as atomic and molecular wires bridging metal electrodes.⁴⁵

IV. SUMMARY

Altermagnets like antiferromagnets have no macroscopic magnetization, but unlike antiferromagnets they exhibit spin-split band structures. The differences between the properties of altermagnetic and antiferromagnetic crystals have been attributed to differing symmetry operations connecting the crystal sublattices of opposite spin in these materials.

This paper explores theoretically for the first time the transport properties of altermagnetic quantum dots with $C_4\mathcal{T}$ symmetries and compares them with those of their antiferromagnetic twins with \mathcal{IT} symmetries. For quantum dots that (together with conducting leads connected to them) obey these symmetries this work makes the following predictions:

1. The anomalous Hall effect, including giant anomalous Hall resistance in the tunneling regime, is predicted for antiferromagnetic dots but not for altermagnetic dots.
2. The spin-Hall effect is predicted for both antiferromagnetic and altermagnetic dots, excepts for those with mirror symmetries.
3. Spin filtering (in two terminal arrangements where the Hall voltage leads are decoupled from the dot but nothing else is changed) is predicted for altermagnetic dots but not for antiferromagnetic dots.

These predictions have been made above for examples of quantum dot geometries based on the 1/5-depleted square lattice, the square-octagon lattice and the Lieb lattice with armchair, zigzag, square or octagon edges and various lead arrangements, all conforming to $C_4\mathcal{T}$ or \mathcal{IT} symmetries.

If the relevant $C_4\mathcal{T}$ or \mathcal{IT} symmetries and all mirror symmetries are broken by disorder in the dot and/or by the arrangement chosen for the leads then the present work predicts both the altermagnetic and antiferromagnetic dot to exhibit the anomalous Hall effect, including giant anomalous Hall resistance in the tunneling regime, the spin-Hall effect and two terminal spin filtering. I.e., symmetry breaking blurs the qualitative differences between the transport properties of altermagnetic and antiferromagnetic quantum dots.

ACKNOWLEDGMENTS

This research was supported by the Digital Research Alliance of Canada.

¹ For a review of altermagnetism see L. Bai, W. Feng, S. Liu, L. Šmejkal, Y. Mokrousov, and Y. Yao, *Altermagnetism: Exploring new frontiers in magnetism and spintronics*, *Adv. Funct. Mater.* **34**, 2409327 (2024).

² L. Šmejkal, J. Sinova, T. Jungwirth, *Emerging Research Landscape of Altermagnetism*, *Phys. Rev. X* **12**, 040501 (2022)

³ L. Šmejkal, J. Sinova, T. Jungwirth, *Beyond Conventional Ferromagnetism and Antiferromagnetism: A Phase with Nonrelativistic Spin and Crystal Rotation Symmetry*, *Phys. Rev. X* **12**, 031042 (2022)

⁴ Z. Xiao, J. Zhao, Y. Li, R. Shindou, Z.-D. Song, *Spin Space Groups: Full Classification and Applications*, *Phys. Rev. X* **14**, 031037 (2024)

⁵ X. Chen, J. Ren, Y. Zhu, Y. Yu, A. Zhang, P. Liu, J. Li, Y. Liu, C. Li, Q. Liu, *Enumeration and Representation Theory of Spin Space Groups*, *Phys.*

Rev. X **14**, 031038 (2024)

⁶ Y. Jiang, Z. Song, T. Zhu, Z. Fang, H. Weng, Z.-X. Liu, J. Yang, and C. Fang, *Phys. Rev. X* **14**, 031039 (2024)

⁷ X. Zhu, X. Huo, S. Feng, S.-B. Zhang, S. A. Yang, H. Guo, *Design of Altermagnetic Models from Spin Clusters*, *Phys. Rev. Lett.* **134**, 166701 (2025)

⁸ Y. Che, H. Lv, X. Wu, J. Yang, *Engineering Altermagnetic States in Two-Dimensional Square Tessellations* *Phys. Rev. Lett.* **135**, 036701 (2025)

⁹ S. S. Fender, O. Gonzalez, and D. K. Bediako, *Altermagnetism: A chemical perspective*, *J. Am. Chem. Soc.* **147**, 2257 (2025)

¹⁰ N. J. Ghimire, A. S. Botana, J. S. Jiang, J. J. Zhang, Y. S. Chen, J. F. Mitchell, *Large anomalous Hall effect in the chiral-lattice antiferromagnet*

CoNb₃S₆, *Nat. Commun.* **9**, 3280 (2018).

- ¹¹ L. Šmejkal, R. González-Hernández, T. Jungwirth, J. Sinova, Crystal time-reversal symmetry breaking and spontaneous Hall effect in collinear antiferromagnets, *Sci. Adv.* **6** eaaz8809 (2020).
- ¹² M. Naka, S. Hayami, H. Kusunose, Y. Yanagi, Y. Motome, H. Seo, Anomalous Hall effect in κ -type organic antiferromagnets *Phys. Rev. B* **102** 075112 (2020)
- ¹³ H. Reichlová, R. Lopes Seeger, R. González-Hernández, I. Kounta, R. Schlitz, D. Kriegner, P. Ritzinger, M. Lammel, M. Leiviskä, V. Petříček, P. Doležal, E. Schmoranzerová, A. Bad'ura, A. Thomas, V. Baltz, L. Michez, J. Sinova, S. T. B. Goennenwein, T. Jungwirth, L. Šmejkal, Macroscopic time reversal symmetry breaking by staggered spin-momentum interaction, arXiv:2012.15651 (2020)
- ¹⁴ Z. X. Feng, X. R. Zhou, L. Šmejkal, L. Wu, Z. W. Zhu, H. X. Guo, R. González-Hernández, X. N. Wang, H. Yan, P. X. Qin, X. Zhang, H. J. Wu, H. Y. Chen, Z. Meng, L. Liu, Z. C. Xia, J. Sinova, T. Jungwirth, Z. Q. Liu, An anomalous Hall effect in antermagnetic ruthenium dioxide, *Nat. Electron.* **5**, 735 (2022)
- ¹⁵ M. Naka, Y. Motome, H. Seo, Anomalous Hall effect in antiferromagnetic perovskites, *Phys. Rev. B* **106**, 195149 (2022)
- ¹⁶ R. D. Gonzalez Betancourt, J. Zubáč, R. Gonzalez-Hernandez, K. Geishendorf, Z. Šobáň, G. Springholz, K. Olejník, L. Šmejkal, J. Sinova, T. Jungwirth, S. T. B. Goennenwein, A. Thomas, H. Reichlová, J. Železný, D. Kriegner, Spontaneous Anomalous Hall Effect Arising from an Unconventional Compensated Magnetic Phase in a Semiconductor, *Phys. Rev. Lett.* **130**, 036702 (2023)
- ¹⁷ T. P. T. Nguyen, K. Yamauchi, *Ab initio* prediction of anomalous Hall effect in antiferromagnetic CaCrO₃, *Phys. Rev. B* **107**, 155126 (2023)
- ¹⁸ X. Y. Hou, H. C. Yang, Z. X. Liu, P. J. Guo, Z. Y. Lu, Large intrinsic anomalous Hall effect in both Nb₂FeB₂ and Ta₂FeB₂ with collinear antiferromagnetism, *Phys. Rev. B* **107**, L161109 (2023)
- ¹⁹ A. Fakhredine, R. M. Sattigeri, G. Cuono, C. Autieri, Interplay between altermagnetism and nonsymmorphic symmetries generating large anomalous Hall conductivity by semi-Dirac points induced anticrossings, *Phys. Rev. B* **108**, 115138 (2023)
- ²⁰ M. Wang, K. Tanaka, S. Sakai, Z. Wang, K. Deng, Y. Lyu, C. Li, D. Tian, S. Shen, N. Ogawa, N. Kanazawa, P. Yu, R. Arita, F. Kagawa, Emergent zero-field anomalous Hall effect in a reconstructed rutile antiferromagnetic metal, *Nat. Commun.* **14**, 8240 (2023)
- ²¹ M. Leiviskä, J. Rial, A. Bad'ura, R. L. Seeger, I. Kounta, S. Beckert, D. Kriegner, I. Joumard, E. Schmoranzerová, J. Sinova, O. Gomonay, A. Thomas, S. T. B. Goennenwein, H. Reichlová, L. Šmejkal, L. Michez, T. Jungwirth, V. Baltz, Anisotropy of the anomalous Hall effect in thin films of the altermagnet candidate Mn₅Si₃, *Phys. Rev. B* **109**, 224430 (2024)
- ²² L. Sheng, C. S. Ting, Intrinsic spin Hall effect in mesoscopic systems, *International Journal of Modern Physics B* **20**, 2339 (2006)
- ²³ M. Naka, S. Hayami, H. Kusunose, Y. Yanagi, Y. Motome, H. Seo, Spin current generation in organic antiferromagnets, *Nat. Commun.* **10**, 4305 (2019).
- ²⁴ H.-Y. Ma, M. Hu, N. Li, J. Liu, W. Yao, J.-F. Jia, J. Liu, Multifunctional antiferromagnetic materials with giant piezomagnetism and noncollinear spin current, *Nat. Commun.* **12**, 2846 (2021).
- ²⁵ R. González-Hernández, L. Šmejkal, K. Výborný, Y. Yahagi, J. Sinova, T. Jungwirth, J. Železný, Efficient Electrical Spin Splitter Based on Non-relativistic Collinear Antiferromagnetism, *Phys. Rev. Lett.* **126**, 127701 (2021).
- ²⁶ M. Naka, Y. Motome, H. Seo, Perovskite as a spin current generator, *Phys. Rev. B* **103**, 125114 (2021)
- ²⁷ H. Bai, L. Han, X. Y. Feng, Y. J. Zhou, R. X. Su, Q. Wang, L. Y. Liao, W. X. Zhu, X. Z. Chen, F. Pan, X. L. Fan, C. Song, Observation of Spin Splitting Torque in a Collinear Antiferromagnet RuO₂, *Phys. Rev. Lett.* **128**, 197202 (2022)
- ²⁸ A. Bose, N. J. Schreiber, R. Jain, D.-F. Shao, H. P. Nair, J. Sun, X. S. Zhang, D. A. Muller, E. Y. Tsymbal, D. G. Schlom, D. C. Ralph, Tilted spin current generated by the collinear antiferromagnet ruthenium dioxide, *Nat. Electron.* **5**, 267 (2022)
- ²⁹ S. Karube, T. Tanaka, D. Sugawara, N. Kadoguchi, M. Kohda, J. Nitta, Observation of Spin-Splitter Torque in Collinear Antiferromagnetic RuO₂, *Phys. Rev. Lett.* **129**, 137201 (2022)
- ³⁰ H. Bai, Y. C. Zhang, Y. J. Zhou, P. Chen, C. H. Wan, L. Han, W. X. Zhu, S. X. Liang, Y. C. Su, X. F. Han, F. Pan, C. Song, Efficient spin-to-charge conversion via altermagnetic spin splitting effect in antiferromagnet RuO₂, *Phys. Rev. Lett.* **130**, 216701 (2023)
- ³¹ X. Chen, D. Wang, L. Li, B. Sanyal, Giant spin-splitting and tunable spin-momentum locked transport in room temperature collinear antiferromagnetic semimetallic CrO monolayer, *Appl. Phys. Lett.* **123**, 022402 (2023).
- ³² J. Sinova, S. O. Valenzuela, J. Wunderlich, C. H. Back, T. Jungwirth, Spin Hall effects *Rev. Mod. Phys.* **87**, 1213 (2015)
- ³³ A. Mook, R. R. Neumann, A. Johansson, J. Henk, I. Mertig, Origin of the magnetic spin Hall effect: Spin current vorticity in the Fermi sea, *Phys. Rev. Research* **2**, 023065 (2020)
- ³⁴ Q. R. Cui, Y. M. Zhu, X. Yao, P. Cui, H. X. Yang, Giant spin-Hall and tunneling magnetoresistance effects based on a two-dimensional nonrelativistic antiferromagnetic metal, *Phys. Rev. B* **108**, 024410 (2023)
- ³⁵ Y. Zhang, H. Bai, L. Han, C. Chen, Y. Zhou, C. H. Back, F. Pan, Y. Wang, C. Song, Simultaneous High Charge-Spin Conversion Efficiency and Large Spin Diffusion Length in Altermagnetic RuO₂ *Adv. Funct. Mater.* **34**, 2313332 (2024)
- ³⁶ Z. Zhang, Y. Bai, X. Zou, B. Huang, Y. Dai, C. Niu, Altermagnetic quantum spin Hall effect in a Chern homobilayer *Phys. Rev. B* **112**, 085128 (2025)
- ³⁷ C. Sun, J. Linder, Spin pumping from a ferromagnetic insulator into an altermagnet, *Phys. Rev. B* **108**, L140408 (2023)
- ³⁸ Y. Che, H. Lv, X. Wu, J. Yang, Realizing altermagnetism in two-dimensional metal-organic framework semiconductors with electric-field-controlled anisotropic spin current, *Chem. Sci.* **15**, 13853 (2024)
- ³⁹ E. W. Hodt, J. Linder, Spin pumping in an altermagnet/normal-metal bilayer, *Phys. Rev. B* **109**, 174438 (2024)
- ⁴⁰ M. Büttiker, Four-Terminal Phase-Coherent Conductance, *Phys. Rev. Lett.* **57**, 1761 (1986)
- ⁴¹ D. S. Fisher and P. A. Lee, Relation between conductivity and transmission matrix, *Phys. Rev. B* **23**, 6851 (1981)
- ⁴² E. N. Economou and C. M. Soukoulis, Static Conductance and Scaling Theory of Localization in One Dimension, *Phys. Rev. Lett.* **46**, 618 (1981)
- ⁴³ B. M. Bode, M. S. Gordon, Macmolpt: a graphical user interface for GAMESS, *J. Mol. Graphics and Modeling* **16**, 133 (1998).
- ⁴⁴ M. Azari and G. Kirczenow, Gate-tunable valley currents, non-local resistances and valley accumulation in bilayer graphene nanostructures, *Phys. Rev. B* **95**, 195424 (2017)
- ⁴⁵ G. Kirczenow, in *The Oxford Handbook of Nanoscience and Technology, Volume I: Basic Aspects*, edited by A. V. Narlikar and Y. Y. Fu, Chap. 4 (Oxford University Press, Oxford, 2010)